# Retinoid X receptor gamma signaling accelerates CNS remyelination

Jeffrey K Huang, Andrew A Jarjour, Brahim Nait Oumesmar, Christophe Kerninon, Anna Williams, Wojciech Krezel, Hiroyuki Kagechika, Julien Bauer, Chao Zhao, Anne Baron-van Evercooren, et al.

# Retinoid X receptor gamma signaling accelerates CNS remyelination

Jeffrey K. Huang[1]*, Andrew A. Jarjour[2]*, Brahim Nait Oumesmar[3], Christophe Kerninon[3], Anna Williams[2], Wojciech Krezel[4], Hiroyuki Kagechika[5], Julien Bauer[6], Chao Zhao[1], Anne Baron-Van Evercooren[3], Pierre Chambon[4], Charles ffrench-Constant[2], Robin J. M. Franklin[1]

*[1] MRC Centre for Stem Cell Biology and Regenerative Medicine and Department of Veterinary Medicine, University of Cambridge, Madingley Road, Cambridge CB3 0ES, UK*

*[2] MRC Centre for Regenerative Medicine and MS Society/University of Edinburgh Centre for Translational Research, Centre for Inflammation Research, The Queen's Medical Research Institute, 47 Little France Crescent, Edinburgh, EH16 4TJ, UK*

*[3] Centre de Recherche de l'Institut du Cerveau et de la Moelle Epinière, Inserm U.975 ; Université Pierre et Marie Curie-Paris 6 UMR-S975; Cnrs UMR 7225; and AP-HP Groupe Hospitalier Pitié-Salpêtrière, Fédération de Neurologie, 105 bd. de l'Hôpital, 75634 Paris cedex 13, France.*

*[4] Institut de Génétique et de Biologie Moléculaire et Cellulaire (IGBMC), Department of Cell Biology and Development, 1 rue Laurent Fries, BP 10142, 67404 Illkirch, France*

*[5] Graduate School of Biomedical Science, Institute of Biomaterials and Bioengineering, Tokyo Medical and Dental University, 2-3-10 Kanda-Surugadai, Chiyoda-ku, Tokyo 101-0062, Japan*

*[6] Department of Pathology, University of Cambridge, Tennis Court Road, Cambridge CB2 1QP, UK*

**Joint corresponding authors**

Prof. Robin Franklin,
Tel: +44 1223 337642
Email: rjf1000@cam.ac.uk

Prof. Charles ffrench-Constant,
Tel: +44 131 242 6684
Email: cffc@ed.ac.uk

* JKH and AAJ contributed equally to this work

**ABSTRACT**

The molecular basis of CNS myelin regeneration (remyelination) is poorly understood. Here we generate a comprehensive transcriptional profile of the separate stages of spontaneous remyelination following focal demyelination in the rat CNS and show transcripts encoding retinoid acid receptor RXR-gamma is highly differentially expressed during remyelination. We find that oligodendrocyte lineage cells express RXR-gamma in rat tissues undergoing remyelination and in active and remyelinated MS lesions. RXR-gamma knockdown by RNA interference or RXR-specific antagonists severely inhibit oligodendrocyte differentiation in culture. In RXR-gamma deficient mice, adult oligodendrocyte precursor cells efficiently repopulate lesions following demyelination, but display delayed differentiation into mature oligodendrocytes. Administration of the RXR agonist 9-*cis*-retinoic acid to demyelinated cerebellar slice cultures and to aged rats following demyelination results in more remyelinated axons. RXR-gamma is therefore a positive regulator of endogenous oligodendrocyte precursor cell differentiation and remyelination, and may be a pharmacological target for CNS regenerative therapy.

## INTRODUCTION

Following acute demyelination in the central nervous system (CNS), adult oligodendrocyte precursor cells (OPCs) can migrate to the area of injury, differentiate into oligodendrocytes, and restore myelin sheaths[1-3]. However, this natural regenerative process, or spontaneous remyelination, is limited in demyelinating diseases such as multiple sclerosis (MS)[4,5], due in part to the failure of adult OPC differentiation into myelinating oligodendrocytes[6-8]. The failure to restore CNS myelin after injury compromises axonal integrity and leaves them vulnerable to degeneration[9]. While genes regulating OPC proliferation and differentiation in development are intensively studied, relatively little is known regarding the molecular signals regulating adult OPC function following demyelination. The identification of critical signaling networks associated with remyelination would improve the understanding of OPC function in response to injury, and aid in the identification of pharmacological targets for the development of regenerative therapeutics to encourage myelin regeneration[10].

By using a well-established and highly tractable toxin-induced demyelination method in rats[11], combined with laser capture microdissection (LCM) and microarray analysis of selectively isolated lesions, we have generated a complete transcriptome of the separate stages of spontaneous CNS remyelination. We found the transcript encoding retinoid X receptor gamma, or RXR-$\gamma$ was significantly upregulated at the regenerative phase of remyelination, and detected in oligodendrocyte lineage cells of remyelinating lesions in rat CNS and in MS tissues. By using pharmacological and genetic manipulation methods, we found that RXR activation stimulated

oligodendrocyte differentiation to enhance remyelination, thus uncovering a novel role for RXR signaling as a regenerative therapeutic target to promote CNS remyelination in the demyelinated brain.

## RESULTS

### Increased *Rxrg* transcripts in CNS remyelinating lesions

Focal demyelinations were induced in the rat caudal (inferior) cerebellar peduncle (CCP)[12], and lesioned tissues were isolated at 5, 14 and 28 dpl using LCM. For microarray analysis, three independently lesioned rats per time point were used, providing three biological replicates. Labeled RNAs were hybridized onto the Illumina Rat RefSeq chip containing over 22,000 genes, and analyzed using the Illumina BeadStudio and R statistical tools (lumi, limma and fspma package). We identified a total of 8,754 differentially expressed genes (3,197 genes, $P < 0.05$) over the three post lesion time points (**Fig. 1a** and **Supplementary Table 1**). The most highly expressed genes at 5 dpl compared to 14 or 28 dpl were associated with inflammation, including *Mmp7*, *Cxcl13*, and *Arg1*, whereas most of the top genes detected at 14 dpl compared to 5 dpl were associated with myelination, including *Tspan2*, *Mal*, *Edg2*, *Mobp* and *Mog* ($P < 0.05$, **Fig. 1b**). Indeed, an analysis of known genes involved in myelination revealed that most had increased expression from 5 to 14 and 28 dpl (**Fig. 1c**). We also found that genes specific to the OPC lineage such as *Nkx2.2* and *Myt1* displayed decreased expression from 5 to 14 dpl, suggesting that the OPC population has undergone differentiation into oligodendrocytes by 14 dpl.

We next performed Ingenuity Pathway Analysis (IPA) by submitting the list of differentially expressed genes between 5 and 14 dpl, and between 14 and 28 dpl to elucidate the overall physiology of remyelination and active signaling pathways associated with each regeneration time point. We found the top physiological systems networks at 5 dpl, based on genes that displayed higher expression at 5 dpl than 14 dpl, involved the immune response, indicating active inflammation (**Fig. 1d** and **Supplementary Table 2**). Moreover, the top networks at 14 and at 28 dpl, based on genes upregulated at 14 dpl compared to 5 dpl, and 28 dpl compared to 14 dpl, involved nervous system development and function and less immune response, indicating increasing remyelination activity. The most significant pathways detected at 5 dpl are associated with macrophage and inflammation activities, such as Fcγ receptor-mediated phagocytosis in macrophage/monocytes, and interleukin signaling, whereas the most significant signaling pathways at 14 dpl are related to cell metabolism and proliferation/differentiation, such as inositol phosphate metabolism and Notch signaling (**Supplementary Table 3**)**.** These results reveal the overall molecular signature of CNS remyelination involves distinct and temporally regulated signaling pathways characterized by active inflammation at 5 dpl, and initiation of remyelination at 14 dpl.

To identify potentially novel genes that play a role in CNS remyelination, we performed a volcano plot analysis by plotting the fold change ($\log_2$ FC) of differentially expressed genes between 5 and 14 dpl against their significance level (log P-value). We hypothesize, based on our transcriptome analysis that gene pathways upregulated or enriched at 14 dpl likely function to stimulate remyelination

(i.e. OPC differentiation). We found that retinoid X receptor gamma (*Rxrg*) is one of the most significantly upregulated genes at 14 dpl ($\log_2$ FC = 3.375; log P-value = 2.708), and co-clustered with many genes involved in myelination (**Fig. 1e** and **Supplementary Table 4**). RXR-γ and with the other RXR members, RXR-α and RXR-β, are nuclear receptors that function through heterodimeric association with other nuclear receptors, such as retinoic acid receptors (RAR), thyroid hormone receptors (TR), vitamin D receptors (VDR), peroxisome proliferator activator receptors (PPAR) and liver X receptors (LXR) to regulate cell proliferation, differentiation and apoptosis[13]. We found that *Rxra* and *Rxrb* were also differentially expressed over the 3 postlesion timepoints in our remyelination transcriptome, although at lower fold change than *Rxrg*. We also detected the differential expression of genes known to heterodimerize with RXR[14], including *Thra*, *Thrb, Nr1h3* (LXRalpha), *Nr2f1* (COUP-TFI) and *Nr4a2* (Nurr1), supporting a role for RXR signaling in remyelination (**Supplementary Table 5**). Moreover, IPA analysis on the full list of differentially expressed genes from all three post-lesion timepoints revealed an enrichment of pathways associated with RXR signaling (**Table 1**, **Supplementary Fig. 1** and **Supplementary Table 6**), suggesting RXR signaling is highly active in lesions and might play a role in remyelination.

To validate RXR expression in remyelination, we performed real time quantitative polymerase chain reaction (qPCR) on reverse transcribed mRNAs isolated from non-lesioned, 5 dpl, 14 dpl and 28 dpl CCPs by laser capture microdissections (**Fig. 1 f**). We found that *Rxra*, *Rxrb* and *Rxrg* expressions were concordant with their differential expressions *in silico*. In particular, *Rxrg* was barely expressed at 5 dpl, but dramatically increased expression, by nearly 8-fold at 14 dpl, and remained

highly expressed at 28 dpl. Moreover, *in situ* hybridization analysis on focally demyelinated rat brains revealed the density of *Rxrg* expressing cells in lesions was at least 3 times greater at 14 and 28 dpl than at 5 dpl (**Figs. 1g** and **h**), supporting its active expression at the onset of remyelination

**RXR-γ expression in oligodendrocyte lineage cells**

The remyelination environment is recognized by activated adult OPCs, regenerated oligodendrocytes, microglia/macrophage, and reactive astrocytes[15]. To determine which cells displayed RXR-γ activity, we performed immunfluorescence analysis on focally demyelinated rat brains. RXR-γ was detected predominantly in the cytosol of $ED1^+$ macrophages (**Fig. 2a**) and rarely in reactive astrocytes (**Fig. 2b**). RXR-γ was also in the cytosol of $Nkx2.2^+$ OPCs (**Fig. 2c**) and in the nuclei of $CC1^+$ oligodendrocytes (**Fig. 2d**), suggesting it may be translocated to influence OPC differentiation. In non-lesioned white matter, RXR-γ was faintly detectable in $CC1^+$ oligodendrocytes (**Fig. 2e**). In non-lesioned gray matter, RXR-γ was most strongly expressed in neurons, such as in the striatum (**Fig. 2f**). These results confirm RXR-γ is highly expressed in the injury environment. To determine what percentage of total RXR-$\gamma^+$ cells in lesions are oligodendrocyte lineage cells, we performed *in situ* hybridization against *Rxrg* followed by immunoperoxidase stain using antibodies against Olig2 (**Supplementary Fig. 2**). We found that oligodendrocyte lineage cells ($Olig2^+$ RXR-$\gamma^+$) represent approximately 8.7% of total RXR-$\gamma^+$ cells at 5 dpl, 21.5% at 14 dpl, and 25.5% at 28 dpl (**Fig. 2g**), suggesting the majority of RXR-$\gamma^+$ cells might be expressed by macrophages. When we quantitated the number of RXR-$\gamma^+$ oligodendrocytes in lesions, we found the RXR-$\gamma^+CC1^+$ cells increased significantly

from 5 dpl to 14 dpl and 28 dpl, suggesting increasing OPC differentiation in lesions over time (**Fig. 2h**).

Several independent lines of evidence suggest that RXR-γ may play a role in remyelination. Following spinal cord contusions, all three RXR isoforms become actively expressed by reactive microglia, neurons, astrocytes, and oligodendrocytes in the cytosol, suggesting RXR signaling is involved in the injury response of the damaged CNS[16]. Moreover, only RXR-γ was observed to translocate from the oligodendrocyte cytosol to the nucleus after injury[16]. We have also performed a database search through the recent detailed microarray analysis of purified oligodendrocyte lineage cells and found that RXR-γ is significantly enriched in purified OPCs[17]. To confirm that nuclear expression of RXR-γ correlates with OPC differentiation and myelination, immunostaining analysis was performed on purified OPC/dorsal root ganglion co-cultures. After two days in co-culture, RXR-γ was detected predominantly in the cytosol of oligodendrocyte precursor cell bodies and processes (**Fig. 2i**). However, as these cells differentiate and begin to myelinate, RXR-γ was no longer detected in the processes and became restricted to the cell bodies and nuclei (**Figs. 2j** and **k**), suggesting RXR-γ redistributes to the nucleus during OPC differentiation.

**RXR-γ is differentially distributed in MS brain lesions**

To examine RXR-γ expression in MS lesions, immunostaining analyses were performed on snap-frozen post-mortem brain sections from randomly chosen MS cases, including secondary progressive (SP, 2 cases) and relapsing remitting (RR, 1 case) and from 3 non-neurological controls (**Supplementary Table 7**). In active

borders of MS lesions, RXR-γ expression was detected in either the nucleus or cytosol of oligodendrocyte lineage cells (**Fig. 3a**–**d**). A quantification of RXR-$\gamma^+$ expression in these lesions revealed that 84.5 ± 5.7% of these cells displayed nuclear Olig1$^+$ expression, indicating that RXR-γ is expressed by activated OPCs that have likely migrated to lesions in response to demyelination in MS. RXR-γ was also detected in activated microglia/macrophages (**Fig. 3e**) and reactive astrocytes (**Fig. 3f**).

To determine the density of cells expressing RXR-γ in active vs. inactive area of damage, Luxol fast blue (LFB) stain was performed on MS brain sections followed by immunoperoxidase staining with the macrophage/monocyte marker MHCII to differentiate the active border (LFB$^+$ MHCII$^+$) from the chronic inactive core (LFB$^-$ MHC$^{+/-}$) of lesions (**Fig. 3g**). We also quantified the number of RXR-$\gamma^+$ cells in the peri-plaque white matter (PPWM) surrounding the lesion, a remyelinated shadow plaque lesion (RM), and in control normal appearing white matter from non-neurological cases (control WM). We found that active lesions and PPWM exhibited significantly greater density of RXR-$\gamma^+$ cells than control WM (**Fig. 3h**). By contrast, chronic inactive core lesions exhibited significantly fewer RXR-$\gamma^+$ cells than NAWM. We also detected significantly more nuclear than cytoplasmic RXR-γ expression in active lesions, PPWM and the remyelinated shadow plaque (> 4 fold) compared to chronic inactive cores. In contrast to the MS lesions, we detected significantly more cytoplasmic than nuclear RXR-γ expression (> 2 fold) in the control white matter, suggesting RXR-γ may be sequestered in the cytoplasm of terminally differentiated cells in normal adult CNS. The detection of nuclear RXR-γ in active lesions, shadow plaque and PPWM suggests these are areas of high cellular activity possibly

associated with repair. Moreover, the diminished expression of RXR-γ in chronic inactive lesions correlates well with the impairment of remyelination in the progressive stages of MS, thus supporting a role for RXR signaling in repairing demyelinated CNS axons.

**RXR-γ loss-of-function impairs OPC differentiation**

To determine if RXR-γ regulates OPC differentiation, we transfected cultured OPCs with non-targeting siRNAs as control (**Fig. 4a**), siRNAs generated against *Rxra* (**Fig. 4b**), or *Rxrg* (**Fig. 4c**). After 72 hours in differentiation media, RXR-γ siRNA transfected oligodendrocytes were less morphologically differentiated compared to controls. We immunostained oligodendrocyte lineage cells with anti-O4 and anti-MBP antibodies, and determined the differentiation state of oligodendrocyte lineage cells based on their morphologies as defined by multiple process outgrowth (*simple*), extensive process outgrowth and branching (*complex*), and terminal membrane expansion (*membrane*) (**Fig. 4d**). We found that control non-targeting siRNAs did not influence OPC differentiation, as the percentage of $O4^+$ oligodendrocytes displaying the simple, complex or membrane morphologies appeared similar to those observed in mock, non-transfected oligodendrocytes (**Fig. 4d**). By contrast, cells transfected with RXR-γ siRNAs displayed a significant increased in oligodendrocytes displaying simple morphologies, and a dramatic reduction in complex morphologies, indicating a failure to achieve efficient differentiation. We also found that cells transfected with RXR-α siRNAs exhibited decreased $MBP^+$ membrane sheets, although not as severely as cells transfected with RXR-γ siRNAs. Moreover, the percentage of $MBP^+$ cells decreased by more than 30% in RXR-α or RXR-γ siRNA transfected cells compared to controls (**Supplementary Fig. 3**). Immunostaining

analysis revealed that oligodendrocyte lineage cells expressed both RXR-α and RXR-γ, but barely any RXR-β in culture (**Supplementary Fig. 3**). Western blot analysis confirmed the siRNAs specifically knocked down RXR-α and RXR-γ expressions, respectively, and did not interfere with the expression of other RXR members (**Fig. 4e** and **Supplementary Fig. 4**). These results suggest both RXR-α and RXR-γ are involved in stimulating oligodendrocyte differentiation.

Previous studies have shown that mice lacking RXR-γ do not display any gross abnormalities during development and are viable after birth[18]. However in adults, these mutants display thyroid hormone resistance, changes in their metabolic activity, and depressive behaviors via reduced dopaminergic signaling[19-21], suggesting RXR-γ regulates homeostatic functions in the adult CNS. To determine if CNS remyelination requires RXR-γ, we performed focal demyelination on *Rxrg*$^{-/-}$ mice by lysolecithin injection into the spinal cord ventral funiculus of adult mice and anlaysed spinal cord lesions at 15 and 30 dpl. At 15 dpl, we found the density of ED1$^{+}$ macrophages/activated microglia, GFAP$^{+}$ reactive astrocytes, and Olig2$^{+}$ oligodendrocyte lineage cells were not significantly different in the lesions of *Rxrg*$^{-/-}$ mice compared to controls (**Fig. 4f–h**; **Supplementary Fig. 5**), suggesting RXR-γ was not required for their recruitment into lesions. Moreover, there was no obvious difference between the two groups regarding oligodendrocyte lineage cell survival at lesions (**Supplementary Fig. 5**). By contrast, we found a reduction in the number of CC1$^{+}$ oligodendrocytes in the lesions of *Rxrg*$^{-/-}$ animals compared to control (**Fig. 4f–h**). However, this decrease appeared to be transient since by 30 dpl the number of CC1$^{+}$ cells in *Rxrg*$^{-/-}$ mice had increased in lesions, almost to the level observed in control mice (**Fig. 4h**). We also detected more Nkx2.2$^{+}$ OPCs in *Rxrg*$^{-/-}$ animals

compared to control at 15 and 30 dpl, suggesting OPCs were less efficient at differentiating into oligodendrocytes. We next performed semi-thin resin section analysis and found no obvious difference in remyelination between *Rxrg*$^{-/-}$ and control mice at 30 dpl (**Supplementary Fig. 5**). These results suggest the loss of RXR-γ impairs OPC differentiation after demyelination, but possible compensatory mechanisms may eventually overcome the absence of RXR-γ signaling to regenerate myelinating oligodendrocytes.

**RXR antagonists inhibit OPC differentiation**

To abolish all RXR activity, we treated OPC cultures with the synthetic RXR-selective antagonist, HX531 or PA452[22]. After 72 hours, we immunostained oligodendrocyte lineage cells with antibodies against O4 and MBP, and determined their differentiation states based on their morphologies (**Fig. 5a**). Compared to untreated or control cultures (**Fig. 5b**), we found that increasing concentrations of either HX531 (**Fig. 5c**) or PA452 (**Fig. 5d**) resulted in oligodendrocyte lineage cells displaying more simple morphologies and less membrane morphologies (**Fig. 5e**). Moreover, we found the percentage of total MBP$^{+}$ oligodendrocytes decreased significantly in cells treated with either antagonist compared to controls (**Supplementary Fig. 6**), suggesting RXR antagonists significantly inhibited their differentiation. We did not detect a significant difference in the number of oligodendrocyte lineage cells undergoing apoptosis between antagonist-treated and control cultures (**Supplementary Fig. 7**), indicating that RXR antagonists do not influence their survival and were not toxic at the concentrations analyzed.

The observation that RXR signaling is required for oligodendrocyte lineage cell differentiation in purified OPC cultures raises the question of whether its role also extends to promoting myelin formation. This was addressed by manipulating RXR signaling in OPC-dorsal root ganglion (DRG) neuron co-cultures. The extent of myelination was determined by $MBP^+$ oligodendrocyte-axon contact (*contacting*), oligodendrocyte membrane extension on axons (*extending*) or myelin compaction based on elongated oligodendrocyte membranes over $Caspr^+$ paranodal clusters (*wrapping*) (**Fig. 5f**). We found that administration of HX531 (**Fig. 5g**) or PA452 (**Fig. 5h**) to the co-cultures resulted in a concentration-dependent increase in the number of contacting oligodendrocytes and a dramatic reduction in the percentage of myelinating oligodendrocytes (**Fig. 5k**). To determine if decreased myelination was caused by failed oligodendrocyte differentiation or a potential decrease in the number or axons, we assessed the percentage of total neurofilament-labeled ($NFH^+$) axons that are myelinated. We found the percentage of myelinated axons with respect to total $NFH^+$ axons in the culture decreased significantly when either antagonist was added to the culture media (**Fig. 5l**), suggesting oligodendrocytes were stalled at the premyelinating stage. These results indicate that RXR signaling in oligodendrocytes is likely necessary for efficient myelination.

**9-*cis*-retinoic acid improves CNS remyelination**

9-*cis*-retinoic acid (9cRA), an isomer of the vitamin A-derived all trans retinoic acid, is a known ligand for RXR activation[23]. In a previous study carried out by Pombo et al.[24], 9cRA was shown to activate transcription of the myelin basic protein (MBP) gene, suggesting that RXR signaling may promote OPC differentiation. To assess the role of 9cRA in OPC differentiation, we treated OPC cultures with 9cRA for 48

hours. Since thyroid hormone may influence RXR signaling, we omitted triiodothyronine and thyroxine in the culture medium. Compared to control or untreated cultures (**Fig. 5m**), we found that 50nM 9cRA resulted in increased percentage of $MBP^+$ membrane sheets (**Fig. 5n** and **q**), suggesting that 9cRA promotes OPC differentiation. However, 9cRA is known to activate both RXRs and retinoic acid receptors (RARs)[23]. To determine that the effect of 9cRA on OPC differentiation was dependent on RXR activity, we co-administered 9cRA with the RXR antagonists HX531 (**Fig. 5o**) or PA452 (**Fig. 5p**) to OPC cultures. We found that a low antagonist concentration (0.1 μm HX531 or 0.1 μm PA452) was sufficient to abrogate 9cRA induced OPC differentiation, and that increasing concentration of either antagonist in the presence of 9cRA further decreased the percentage of mature oligodendrocyte membranes (**Fig. 5q**), suggesting that 9cRA stimulates OPC differentiation via RXR signaling. To determine that RXR activation stimulates OPC differentiation, we treated OPC culture with the RXR selective agonist, HX630 or PA024[25,26]. We found that both agonists increased the elaboration of membrane sheets by cultured oligodendrocytes, consistent with the observed response of these cells to 9cRA treatment (**Fig. 5r**). We also examined the effect of 9cRA on myelinating co-cultures but did not observe a significant increase in myelination (**Fig. 5j** and **l**), suggesting that endogenous activation of RXR signaling was sufficient for maximal oligodendrocyte differentiation by 10 days in co-culture, or that 50 nM 9cRA was insufficient to increase differentiation from OPCs.

To determine whether activation of RXR signaling would promote CNS remyelination, we tested the effects of 9cRA on *ex vivo* demyelinated cerebellar slice cultures. Mouse cerebellar slice cultures were treated overnight with lysolecithin

after 14 days *in vitro* as described previously in rats to induce demyelination[27]. Cultures were then maintained in 9cRA or the antagonists HX531 or PA452 for a further 48 hours (**Fig. 6e**) or 14 days (**Fig. 6f**). We found that 9cRA treatment for 48 hours or 14 days did not result in a significant increase in the number of $NG2^+$ OPCs or $MBP^+$ oligodendrocytes, whereas HX531 or PA452 resulted in the significant reduction of $MBP^+$ oligodendrocytes at both time points. However, an analysis of the percentage of myelin ensheathment revealed that 9cRA significantly increased the percentage of $MBP^+$ membranes on $NFH^+$ axons relative to control slices (**Fig. 6g**). Moreover, cell proliferation analysis using BrdU labeling revealed no difference in the density of $BrdU^+$ cells between 9cRA treated cultures compared to control (**Supplementary Fig. 7**), suggesting 9cRA does not appear to affect cell proliferation.

We next asked whether exogenous 9cRA could similarly enhance remyelination *in vivo*. Since retinoids can influence the adaptive immune response[28], direct effects of 9cRA attributable to remyelination would be difficult to distinguish from those that were primarily immunomodulatory. We therefore used the focal toxin-induced model of demyelination for our experiment rather than a variant of experimental autoimmune encephalomyelitis (EAE), a widely used model system for studying the immunological aspects of MS. The toxin model also provides a clear distinction between acute demyelination, whose induction is independent of the adaptive immune system, and subsequent remyelination, allowing the effects of 9cRA on remyelination to be specifically addressed. Furthermore, we performed our studies in aged adult rats where remyelination occurs less efficiently than in young adult rats thereby providing a more clinical relevant context[29]. Following focal demyelination,

10 mg/kg/day of 9cRA or saline were injected intraperitoneally for 14 days from 7 to 21 dpl, and then analyzed the extent of remyelination at 27 dpl. We found the densities of $Olig2^+$ oligodendrocyte lineage cells, and $Nkx2.2^+$ OPCs at lesions in the 9cRA treated group were similar to those observed in the saline treated group (**Fig. 6h**). However, we detected an increase of $CC1^+$ differentiated oligodendrocytes in 9cRA treated group compared to control. Moreover, real time qPCR on laser capture microdissected lesions at 27 dpl resulted in approximately 30% increase of *Mbp* expression, an indicator of myelin regeneration, in 9cRA treated animals compared to control (**Fig. 6i**). We did not observe a significant difference between 9cRA treated and control groups in the expressions of *Pdgfra* or *Scarb1*, which correlates with OPC or macrophage activities, respectively. By semi-thin resin and ultrastructural analyses of CCP lesions at 27 dpl, we found that the 9cRA treated group (**Fig. 6j** and **k**) displayed more remyelinated axons compared to control (**Fig. 6l** and **m**). The improvement of CNS remyelination after 9cRA treatment was confirmed by ranking analysis of the semi-thin resin sections (**Fig. 6n**). We also assessed the efficiency of remyelination by performing a G-ratio analysis, which describes the ratio of axon diameter to myelinated axon. We found that 9cRA treated groups exhibited lower G-ratio compared to saline treated group due to thicker remyelinated sheaths around axons (**Fig. 6o** and **p**), consistent with an acceleration of CNS remyelination.

## DISCUSSION

We have generated a transcriptional database of differentially expressed genes associated with spontaneous CNS remyelination after focal toxin-induced demyelination in the rat white matter. The remyelination transcriptome will be a useful resource for the neuroscience and regenerative medicine community to better understand the signaling networks and factors required to repair the injured brain via endogenous neural precursor cells, as well as how normally expressed genes and signaling pathways in the white matter might be affected in pathologies of CNS demyelination or failed myelin regeneration.

The prominence of RXR signaling pathways in the remyelination transcriptome reveals the association of RXR signaling with the CNS regenerative response, and opens a new area of future research on the role of RXRs in regenerative medicine. In the mammalian brain, RXR-γ is generally expressed at low levels in all glial cells in the non-injured CNS[30], but becomes actively expressed by activated microglia/macrophages, reactive astrocytes and oligodendrocytes after CNS injury[16]. We found that RXR-γ was also expressed after focal demyelination and in active MS lesions, suggesting that RXR-γ is a physiological signal of injury in the acutely lesioned brain. Functional analyses in cultured OPCs using siRNAs against RXR-γ or RXR specific antagonists, and in RXR-γ null mice revealed inefficient oligodendrocyte differentiation, indicating RXR-γ is an important regulator of remyelination. Interestingly in purified human adult OPCs, *RXRG* transcripts were not detected by microarray profiling[31]. We found that OPCs from normal appearing white matter of MS brains exhibited more cytoplasmic than nuclear RXR-γ expression, which suggests *RXRG* might not be actively transcribed in “resting” adult

OPCs, and therefore like in rodents, RXR-γ is likely expressed and activated in response to CNS injury in humans.

The ability for RXR to heterodimerize with a number of nuclear receptors suggests RXR can modulate differential gene expression depending on which receptor it heterodimerizes with and when. RXR can form permissive or non-permissive heterodimers with other nuclear receptors[32]. As we have found that 9cRA stimulates differentiation and enhances CNS remyelination, RXR-γ likely acts though permissive heterodimerization. Candidate permissive heterodimers including LXR and PPAR have been described in oligodendrocyte lineage cells[33-35]. In our microarray data, we did not detect the differential expression of any members of the PPAR family, but detected RXR-α, RXR-β, LXRalpha, COUP-TFI, and Nurr1 as possible permissive RXR-γ heterodimers. However, it remains to be determined which nuclear receptor(s) heterodimerize with RXR-γ in oligodendrocyte lineage cells after demyelination, and what genes are transcribed in response to RXR-γ activation to promote the differentiation of OPCs.

RXR agonists, or rexinoids are widely available and show therapeutic promise for cancer cell differentiation therapy, as well as for the treatment of metabolic diseases[32]. 9cRA has been shown to modulate inflammation in EAE[36], suggesting rexinoids might be useful for the treatment of inflammatory diseases of the nervous system such as MS. We have shown here that rexinoids is also able to stimulate oligodendrocyte differentiation and remyelination in the injured CNS, therefore providing an additional role of rexinoids as potential drugs for regenerative therapy in demyelinating disorders.

**ACKNOWLEDGMENTS**

This work was supported by grants from the United Kingdom Multiple Sclerosis Society (RJMF, CffC), the French MS foundation ARSEP (BNO), the Biotechnology and Biological Sciences Research Council of the United Kingdom (CffC, JB), National Multiple Sclerosis Society (CffC, RJMF, ABVE, BNO), AP-HP Hôpital Pitié-Salpêtrière, Service d'Anatomopathologie Neurologique (BNO) et des Maladies du Système Nerveux (ABVE). AW holds a Wellcome Trust Intermediate Fellowship. AJ holds a Fellowship from Multiple Sclerosis Society of Canada. We thank Dr Danielle Seilhean (Service d'Anatomopathologie Neurologique, G-H Pitié-Salpêtrière, Paris) for classification of MS lesions, the French Brain Bank GIE NeuroCEB (Hôpital Pitié-Salpêtrière, Paris, France) and the United Kingdom MS Society Brain Bank (Prof R Reynolds, Imperial College, London) for supplying MS tissue. All tissues were collected with approval of the French and London Multicentre Research Ethics committees. Animal procedures were performed under a UK Home Office Project License.

**AUTHOR CONTRIBUTIONS**

JKH performed *in vivo* experiments and laser capture microdissections, AJ performed *in vitro* experiments, CZ contributed to *in vivo* experiments, AW performed *ex vivo* experiments. BNO, CK, ABVE performed MS tissue analysis. HK generated

RXR antagonists and agonists. WK and PC generated the RXR-γ mouse mutants. JB and JKH performed bioinformatics. CffC and RJMF oversaw the project.

## FIGURE LEGENDS

**Figure 1.** Differential expression of *Rxrg* in CNS remyelination transcriptome. (**a**) Hierarchical clustering and graphical analysis of differentially expressed genes at 5, 14 and 28 dpl ($P < 0.05$). (**b**) Top 10 most upregulated genes in each timepoint relative to the other timepoints. (**c**) Graphical analysis showing the differential expressions of known genes associated with myelination ($P < 0.05$). (**d**) Top 5 overall physiological functions in lesions at 5, 14, and 28 dpl using Ingenuity pathways analysis of upregulated genes from each timepoint (**e**) Vocano plot (x-axis = $\log_2$ fold change (FC) at 14 dpl compared to 5 dpl; y-axis = $\log_2$ p-value) showing highly differentially expressed genes associated with myelination genes. *Rxrg* (green triangle; x, y = 3.3752, 2.7084) is shown as a highly expressed transcript at 14 dpl compared to 5 dpl. (**f**) Real time qPCR detection of *Rxra*, *Rxrb* and *Rxrg* expressions from laser captured lesions during remyelination (n = 3). *Rxrg* is barely detectable in non-lesioned CCPs and at 5 dpl, and highly expressed at 14 and 28 dpl. (**g**) *In situ* hybridization shows the significant increase of $Rxrg^+$ cells within the CCP at 14 dpl and 28 dpl compared to non-lesioned and 5 dpl CCP. Scale bar = 50 μm. (**h**) Quantification of $Rxrg^+$ cells in lesioned CCPs at 5, 14 and 28 dpl (n = 3 per timepoint). Mean values ± s.e.m. are displayed. *$P < 0.05$, ***$P < 0.001$, 1 way ANOVA.

**Figure 2**. RXR-γ expression by oligodendrocyte lineage cells. Co-immunostaining of RXR-γ (red) and (**a**) ED1, (**b**) GFAP, (**c**) Nkx2.2, (**d**) CC1 (green) in lesions at 14 dpl. (**e**) Faint and cytosolic detection of RXR-$\gamma^+CC1^+$ oligodendrocytes in non-lesioned white matter. (**f**) RXR-$\gamma^+$ neurons in the striatum. Nuclei were visualized with Hoechst

(blue). Scale bar = 25 µm. (**g**) Quantification of total Olig2$^+$ RXR-γ$^+$ oligodendrocyte lineage cells relative to the total number of RXR-γ$^+$ cells in CCP lesions at 5, 14 and 28 dpl. (**h**) Quantification of RXR-γ$^+$CC1$^+$ oligodendrocytes in CCP lesions at 5, 14 and 28 dpl. (**i**–**k**) Detection of RXR-γ (green) in oligodendrocyte lineage cells from OPC/DRG neurons co-cultures at 2 DCC, 6 DCC and 7 DCC. Oligodendrocyte lineage cells were immunolabeled with anti-O4 (red), axons with anti-neurofilament (NFH, blue), and nuclei visualized with Hoechst (violet). Scale bar = 60 µm. Mean values ± s.e.m. are displayed. *P < 0.05, **P < 0.01, ***P < 0.001, 1 way ANOVA.

**Figure 3.** Expression of RXR-γ in MS lesions. Co-immunolabeling for RXR-γ (green and (**a**) MOG, (**b**) Sox10, (**c**) Olig1, (**d**) NOG0-A, (**e**) MHCII and (**f**) GFAP (red) in active MS lesion areas. Nuclei were visualized with Hoechst (blue). (**g**) Luxol fast blue staining followed by anti-MHCII immunoperoxidase labeling showing a typical chronic active MS lesion with active border (A) and chronic inactive core (C), as well as peri-plaque white matter (PPWM) (**h**). Quantification of nuclear and cytoplasmic RXR-γ$^+$cells in MS lesions reveals significantly greater number of nuclear RXR-γ$^+$ cells in active lesions, periplaque white matter and remyelinated shadow plaques compared to chronic inactive lesions and normal appearing white matter from non-neurological cases. Scale bars (a-f) = 50 µm; (g) = 2 mm. Mean values ± s.e.m. are displayed. *P < 0.05, ***P < 0.001, 1 way ANOVA.

**Figure 4.** Loss of RXR-γ function impairs oligodendrocyte differentiation. Purified OPCs transfected with (**a**) non-targeting siRNAs, (**b**) RXRA siRNAs and (**c**) RXR-γ siRNAs and visualized with O4 (red) and MBP (green) antibodies after 72 hours in differentiation media. Scale bar = 25 µm. (**d**) Morphological criteria for the maturation

state of differentiating oligodendrocyte were defined as simple, complex or membrane morphologies. Cells transfected with RXR-γ siRNAs resulted in increased percentage of $O4^+$ oligodendrocytes displaying simple morphologies and decreased percentage of complex membrane morphologies compared to mock treated and non-targeting siRNA transfected cells. (**e**) Western blot demonstrates the specificity of RXR-α or RXR-γ knockdowns. Full length blot presented in **Supplementary Fig. 4**. Ventral spinal cord lesions of (**f**) *Rxrg*$^{+/-}$ and (**g**) *Rxrg*$^{-/-}$ mice stained with antibodies against CC1 (green) and Olig2 (red) at 15 days after demyelination. Nuclei visualized with Hoechst (blue). (**h**) Quantification of oligodendrocyte lineage cells at 15 and 30 dpl shows no difference in the density of total $Olig2^+$ cells between –/– and +/– animals, but a reduction of $CC1^+$ cells and increased Nkx2.2+ cells in lesions of –/– compared to +/– animals. Scale bar = 50 μm. Mean values ± s.e.m. are displayed. *P < 0.05, **P < 0.01, ***P < 0.001, Student's t-test.

**Figure 5**. Rexinoids influence oligodendrocyte differentiation and myelination. (**a**) OPC cultures immunolabeled with anti-O4 (red) and anti-MBP (green) following RXR antagonist treatment for 72 hours. Compared to (**b**) non-treated cells, (**c**) HX531 (2 μM), or (**d**) PA452 (5 μM) treatment resulted in less mature oligodendrocytes. (**e**) Increasing antagonists resulted in decreasing number of membrane sheet-bearing oligodendrocytes. Scale bar = 25 μm. (**f**) Oligodendrocyte-DRG co-cultures maintained for 10 days after addition of OPCs immunolabeled with anti-MBP (green), anti-Caspr (red) and anti-NFH (blue). (**g**) Control co-culture, (**h**) HX531 (2 μM), (**i**) PA452 (5 μM), (**j**) 9cRA (50 nM). Scale bar = 100 μm. (**k**) Increasing antagonist concentration resulted in decreasing $MBP^+$ oligodendrocytes, and (**l**) less

myelination. (**m**) Untreated OPC cultures labeled with anti-O4 and anti-MBP. (**n**) 9cRA alone, co-administration of 9cRA and (**o**) HX531 or (**p**) PA452. (**q**) Quantification showing 50 nM 9cRA increased mature oligodendrocyte membranes, and low concentration of HX531 and PA452 were sufficient to abrogate 9cRA-mediated differentiation. (**r**) Treatment of cultured OPCs with 9cRA, HX630 or PA024 resulted in more oligodendrocyte membrane sheets. Scale bar = 25 μm. Mean values ± s.e.m. are displayed. *P < 0.05 vs. control, **P < 0.005 vs. control, β: P < 0.05 vs. 50 nM 9cRA, ββ: P < 0.005 vs. 50 nM 9cRA, Student's t-test.

**Figure 6.** 9 *cis*-retinoic acid enhances CNS remyelination. (**a**) Control cerebellar slices fixed 10 days after demyelination with lysolecithin and immunolabeled with anti-NFH (red) and anti-MBP (green). (**b**) Remyelination was greater under 9cRA treatment, and deficient under (**c**) HX531 or (**d**) PA452 treatment. Scale bar = 20μm. Quantification of $NG2^+$ and $MBP^+$ cells at (**e**) 48 hours or (**f**) 14 days after treatment. (**g**) Quantification of remyelination after 9cRA addition, and HX531 or PA452 addition at high (H, 2 or 5 μM, respectively) or low (L, 0.2 or 0.5 μM) concentrations. (**h**) Increased $CC1^+$ cells in lesions was detected in 9cRA treated rats. 1 way ANOVA. (**i**) Real time qPCR analysis shows increased *Mbp* expression in 9cRA treated animals. Student's t-test. (**j**) Semi-thin section of a lesioned CCP at 27 dpl after 9cRA treatment. Upper left corner shows normal myelinated axons. To the right is a large area of lesion showing axons outlined by thinly remyelinating membranes and dark macrophages. Scale bar = 50 μm. (**k**) Ultrastructural microscopy (1,500X) shows many remyelinated axons (pink) compared to axons that remained demyelinated. (**l**, **m**) Control animal shows very few visible remyelinated axons. (**n**) Ranking analysis. Highest rank = most remyelination. (**o**) G-ratio analysis

shows lower G-ratio in 9cRA treated compared to control. (**p**) Representative images of myelinated, demyelinated, control remyelinated, and 9cRA remyelinated axons. Mean values ± s.e.m. are displayed. ***P < 0.001, Student's t-test.

## METHODS

### Focal demyelination

Female Sprague Dawley rats aged 3 months old (180 to 210 grams) were used for LCM, *in situ* hybridizations and immunostainings. Rats aged from 9 months to one year old (250 to 300 grams) were used for the 9-*cis*-retinoic acid experiment. All experiments were performed in compliance with UK Home Office regulations and the University of Cambridge. Focal demyelination was induced bilaterally by stereotactically injecting 4.0 μl 0.01 % ethidium bromide (EB) in saline into caudal cerebellar peduncles (CCP). For analysis of *Rxrg*$^{+/-}$ and $^{-/-}$ mutants, adult mice (approximately 6 months old) received 1 μl of 1.0 % lysolecithin injection in the ventral funiculus, and mice were sacrificed at 15 dpl and 30 dpl for analysis.

### Laser capture microdissections and microarrays

Animals (n = 4 per group) were sacrificed at 5, 14 and 28 dpl, and brains isolated and snap frozen. 15 μm cryosections were collected on PEN-membrane slides (P.A.L.M. Cat. No. 1400-1000), fixed in 70% ethanol, stained with 1% toluidine blue and then dehydrated with ethanol and xylene. LCM was performed on PALM MicroBeam. Total RNA was isolated using RNAqueous-Micro (Ambion. Cat. No. AM1931) and used for microarray analysis and qPCR. For microarrays, total RNA from brains (n = 3) isolated from each post lesion time point were amplified once and quantity checked. RNAs were hybridized onto Illumina Rat RefSeq slide, giving 3 biological replicates per time point, and differentially expressed genes were detected simultaneously with the Illumina BeadStation. Full list of genes were deposited in NCBI GEO Acc=GSE24821. Microarray analysis was performed at the Cambridge

Genomic Services (University of Cambridge, UK).

**Microarray and bioinformatics**

The Ratref-12 expression Beadchip was used for the microarray study. The quality of the assay was assessed using the BeadStudio control panel. Raw data were loaded into R using lumi[37], and were filtered using the Illumina detection value. This value is a p-value that results from a statistical test between the beads representing the probes and the negative controls on the array, the lumi default filter counts any probes with a p-value below 0.01 as present. The filtering was performed using the following criteria: any given probe needs to be present on at least one of the replicates at any of the time points. After the data were filtered, they were transformed using variance stabilization and then normalized using quantile normalization in lumi. The data were then analyzed using the R package fspma. This algorithm is designed to perform mixed model ANOVA analysis. The model chosen had two main effects, the time points and samples. The latest was set as a random effect and ranking was performed on the time points. Additional comparisons were done using the R package limma. This package uses linear models to compare groups, and was used to perform pairwise comparisons in order to compare the different time points between them. For both sets of results, the ANOVA and the pairwise comparisons, the P-values have been corrected using FDR. P-value cut off used for the analysis was $p < 0.05$. Genes differentially expressed over three postlesion timepoints from the ANOVA analysis ($P < 0.05$) were submitted to Cluster 3.0 for hierarchical clustering analysis (euclidian distance, centroid linkage clustering) and visualized using Java TreeView. IPA analysis was performed using the Ingenuity Pathways Analysis software.

**Antibodies and reagents**

Primary antibodies for used rodent experiments were mouse A2B5 (Millipore, UK), rabbit anti-Caspr (Abcam, UK), mouse anti-ED1 (Serotec, UK), mouse anti-GFAP (DAKO, UK), rat anti-MBP (Serotec, UK) mouse anti-Nkx2.2 (DHSB, University of Iowa), mouse O4 (Millipore, UK), rabbit anti-Olig2 (Millipore, UK), chicken anti-NFH (Encor Biotechnologies, Florida, USA), rabbit anti-RXRγ (Abcam, UK). For MS tissues, rabbit anti-RXRγ (Abcam, UK), rabbit anti-RXRα (Santa Cruz Biotechnology), rabbit anti-RXRβ (Santa Cruz Biotechnology), mouse monoclonal anti-Olig1 (R&D Systems), polyclonal anti-Sox10 (R&D Systems), polyclonal anti-NOGO-A (Santa-Cruz), anti-MHC class II (mouse IgG1, DAKO), anti-GFAP (mouse IgG1, Millipore).

**Immunohistochemistry**

Rats were anaesthetized and perfused with 4% paraformaldehyde at 5 dpl, 14 dpl and 28 dpl before brains were isolated, postfixed and cryosectioned. 12 μm sections containing lesions were detected by rapid toluidine blue staining and light microscopy examination before collection and storage in -80 °C. Immunoperoxidase staining was performed using the Vectastain ABC Kit (Vector Laboratories, UK). Non-radioactive *in situ* hybridization for RXRγ was performed as described previously[29]. For the generation of the *Rxrg* probe, 669 bp rat *Rxrg* cDNA fragment was isolated as described[38] from cultured OPC cell extracts and subcloned into the $CS2^+$ vector. Antisense *Rxrg* was generated with T7 polymerase after BamH1 linearization. Images were photographed and labeled cells were assessed using Axiovision 4.7.1 software (Zeiss). Statistical analysis was performed using Excel

and Prism Graph Pad.

**Purified rat OPC cultures**

OPC cultures were prepared from neonatal Sprague Dawley rats as described previous[39]. OPCs were seeded on PDL-coated 13 mm glass coverslips, and maintained in SATO medium without thyroxine and thiiodothyronine at 37°C in 7.5% $CO_2$. For differentiation experiments, OPCs were cultured in the presence of 1:1000 DMSO, RXR agonists HX630 or PA024 (at 100nM, or 1μM), 5 or 50 nM 9-*cis*-retinoic acid and/or synthetic RXR antagonists HX531 (at 0.1μM, 1 μM, 2 μM, or 4 μM), or PA452 (at 0.1 μM, 1 μM, 5 μM, or 10 μM). Cultures were fixed for immunofluorescence analysis. Confocal z-stacks were acquired using Leica SPE confocal microscope, and analyzed using Image Pro Plus software (Media Cybernetics, UK). Differentiation was analyzed by scoring cells as having either 'simple' (short, non-interdigitating processes, 'complex' (longer, interdigitating processes, but not membrane sheets), or 'membrane' morphology (processes containing MBP-positive membrane sheets). Three 20x fields from each of four coverslips were analyzed per condition.

**Myelinating rat OPC-DRG neuron co-cultures**

Rat OPC and OPC-DRG co-cultures were prepared as described previously[40], with the following modifications: DRG neuron cultures were prepared from embryonic day 15 (E15) Sprague Dawley rats and cultured at a density of $2x10^5$ cells per 22 mm coverslip. DRGs were maintained in DMEM with 10% FCS and 100 ng/ml NGF (Serotec). DRG cultures were treated with fluorodeoxyuridine (FdU) to remove contaminating cells. After 21 days, $2x10^5$ OPCs were added per coverslip to DRGs,

and co-cultures were maintained for a further 10 days in myelination medium (BME with ITS and Glutamax I supplements, 36 µg/ml glucose, and 0.5% fetal calf serum (all Invitrogen)). In myelination experiments, 1:1000 DMSO, 50 nM 9-*cis*-retinoic acid, HX531 (0.2 or 2 µM), or PA452 (0.5 or 5 µM) were added. Cultures were fixed for immunocytochemistry. Oligodendrocytes were scored for their morphology as 'contacting' (processes touching but not aligning with axons), 'extending' (processes aligned with, but not surrounding axons) or 'wrapping' (MBP and caspr-positive internodes clearly visible). Percentage of axon area myelinated was quantified using Image Pro Plus. For each field analyzed, percentage myelinated area was measured by extracting a mask image representing MBP-NFH colocalization from each layer of a confocal stack, carrying out an 'extended depth of field' projection of these mask images to form a single image representing the total myelinated area throughout the stack, the value of which was obtained using the software. Total myelinated area was then divided by the NFH-immunopositive area measured in that field, multiplied by 100. Three 20x fields from each of four coverslips were analyzed per condition.

**Mouse cerebellar slice cultures**

Remyelinating mouse cerebellar slice cultures were prepared based on previously published methods used for rats. Slices were exposed to control medium, or 50 nM 9cRA or low (0.2 or 0.5 µM) or high (2 or 5 µM) doses of RXR antagonists HX531 and PA452, maintained for a further 14 days, and then processed for immunolabeling. Imaging was carried out as described above for oligodendrocyte cultures and myelinating co-cultures. Myelin was quantified using Image Pro Plus as described for the co-cultures. Two experiments were analyzed in duplicate.

**siRNA transfections**

Following shake-off, OPCs were maintained in SATO medium with pen-strep (Invitrogen), 0.5% FBS and 10 nM PDGF and FGF overnight. Medium was removed and replaced with SATO with 0.5% FBS, and cells transfected with 20 μM siRNA (or mock transfected) using 1% Lipofectamine RNAiMAX transfection reagent (Invitrogen) in OPTI-MEM. siRNA sequences used were obtained from Dharmacon/Thermo Scientific (RXRα: L-089934-01, RXRγ: L-083061-08, Non-targeting: D-001810-10). Medium was replaced with SATO (without T3 or T4) with 0.5% FBS and pen-strep after 6 hours. Cells were maintained in culture for 72 hours, and then fixed with 4% PFA for 20 minutes at 4°C or lysed for 10 minutes on ice with TEN buffer with 1% Triton-X-100 and 1X protease and phosphatase inhibitor cocktails (Calbiochem). Lysates were subjected to SDS-PAGE and western blotting.

**9-*cis* retinoic acid analysis on focal demyelination**

Aged rats (n = 10 per group) with focal demyelinating lesions were injected with 10 mg/kg 9-*cis*-retinoic acid (BIOMOL International, UK) or saline by i.p. from 7 to 21 dpl and sacrificed at 27 dpl for remyelination analysis by microscopy and PCR. For semithin resin sections and electron microscopy, animals (n = 6 per group) were perfused with 4% glutaraldehyde, brains removed, 1 mm transverse cerebellum/brain stem sections obtained, processed through osmium tetroxide, dehydrated in ethanol, and embedded in resin (TAAB Laboratories, UK). 1 μm resin sections were collected on glass slides and stained with 1% toluidine blue. The extent of remyelination was then assessed by light microscopy. For ultrastructural analysis, resin-embedded tissues were cut and examined by Hitachi H-600 Electron Microscope. Ranking analysis (n = 4 per group) was performed using a 2-tailed

Mann Whitney test and analyzed by using Excel and Prism Graph Pad. G-ratio analysis was performed using NIH ImageJ. The remaining animals (n = 4 per group) were sacrificed, brains removed for LCM and qPCR analysis.

**Quantitative PCR**

PCR primers for rat *Mbp*, *Pdgfra*, *Scarb1*, *B2M*, *Rxra*, *Rxrb*, *Rxrg* and *Actin* were purchased from Gene Globe (Qiagen). Real time qPCR was performed with Quanti-Tect SYBR green PCR Kit (Qiagen) and analyzed by Rotor Gene 6000 PCR analyzer (Corbett Research). Results were normalized against *Actin* or *B2M* and expressed as mean ± s.e.m. Statistical analysis was performed using Prism Graph Pad.

**MS tissue samples and immunohistochemistry**

Snap frozen post-mortem MS brain samples were obtained from the French GIE NeuroCEB brain bank (Dr. Danielle Seilhean, Pitié-Salpêtrière Hospital, Paris) and the UK MS tissue Bank (Dr. Richard Reynolds, Imperial College, London). Control brain samples from patients, who had died from non-neurological diseases, were also obtained from the same sources. Tissues were collected with the donors fully informed consent via a prospective donor scheme following ethical approval. Three randomly chosen MS cases (**Supplementary Table 6**) were studied, including secondary progressive (SP, 2 cases) and relapsing remitting (RR, 1 case). For these MS cases, the mean age was 66.3 years (range: 65-74). The death-tissue preservation delay varied between 20 to 45 hours. Histological assessment of the lesions was performed using Luxol fast blue/Cresyl violet and Oil-red-O (macrophages filled with myelin debris) histological staining. MS lesions were

classified according to their inflammatory activity (KP1 immunolabeling) and on the basis of histological criteria of acute (active demyelination, myelin vacuolation, inflammation or edema, minor gliosis and vague margin), chronic lesions (no myelin vacuolation, absence of inflammation, gliosis, axonal loss and sharp margin) and shadow plaques (myelin pallor). The expression of RXR-γ was studied in 6 MS lesions with active border (n = 3), chronic silent core (n = 5), and shadow plaques (n = 1, partially remyelinated).

Snap frozen MS tissue sections were hydrated in PBS and microwaved in Vector unmasking solution, according the manufacturer protocol. Briefly, sections were pre-incubated in blocking buffer (10% NGS, 0.1% Triton-X 100 in PBS) for 1 hour and incubated overnight with primary antibodies at 4°C. After overnight incubation, slides were extensively washed in PBS/0.1% Triton X-100 and incubated with appropriate secondary antibodies. Quantification of $RXR\gamma^+$ cells was performed on ImageJ software of at least 3 serial MS sections (100μm apart) in active borders, chronic silent core and peri-plaque white matter from 3 distinct cases and in the NAWM from non-neurological controls. Data are expressed as the mean ± s.e.m. Non-parametric statistical tests were performed (1 way ANOVA test) and the results were considered significant at $P < 0.05$.

**REFERENCES**


1. Prineas, J.W. & Connell, F. Remyelination in multiple sclerosis. *Ann. Neurol* **5**, 22-31 (1979).
2. Patani, R., Balaratnam, M., Vora, A. & Reynolds, R. Remyelination can be extensive in multiple sclerosis despite a long disease course. *Neuropathol. Appl. Neurobiol* **33**, 277-287 (2007).

3. Raine, C.S. & Wu, E. Multiple sclerosis: remyelination in acute lesions. *J. Neuropathol. Exp. Neurol* **52**, 199-204 (1993).
4. Goldschmidt, T., Antel, J., König, F.B., Brück, W. & Kuhlmann, T. Remyelination capacity of the MS brain decreases with disease chronicity. *Neurology* **72**, 1914-1921 (2009).
5. Franklin, R.J.M. Why does remyelination fail in multiple sclerosis? *Nat. Rev. Neurosci* **3**, 705-714 (2002).
6. Chang, A., Tourtellotte, W.W., Rudick, R. & Trapp, B.D. Premyelinating oligodendrocytes in chronic lesions of multiple sclerosis. *N. Engl. J. Med* **346**, 165-173 (2002).
7. Kuhlmann, T. et al. Differentiation block of oligodendroglial progenitor cells as a cause for remyelination failure in chronic multiple sclerosis. *Brain* **131**, 1749-1758 (2008).
8. Wolswijk, G. Chronic stage multiple sclerosis lesions contain a relatively quiescent population of oligodendrocyte precursor cells. *J. Neurosci* **18**, 601-609 (1998).
9. Nave, K. & Trapp, B.D. Axon-glial signaling and the glial support of axon function. *Annu. Rev. Neurosci* **31**, 535-561 (2008).
10. Fancy, S.P.J. et al. Overcoming remyelination failure in multiple sclerosis and other myelin disorders. *Exp. Neurol* **225**, 18-23 (2010).
11. Blakemore, W.F. & Franklin, R.J.M. Remyelination in experimental models of toxin-induced demyelination. *Curr. Top. Microbiol. Immunol* **318**, 193-212 (2008).
12. Woodruff, R.H. & Franklin, R.J.M. Demyelination and remyelination of the caudal cerebellar peduncle of adult rats following stereotaxic injections of lysolecithin, ethidium bromide, and complement/anti-galactocerebroside: a comparative study. *Glia* **25**, 216-228 (1999).
13. Germain, P. et al. International Union of Pharmacology. LXIII. Retinoid X receptors. *Pharmacol. Rev* **58**, 760-772 (2006).
14. Lefebvre, P., Benomar, Y. & Staels, B. Retinoid X receptors: common heterodimerization partners with distinct functions. *Trends Endocrinol Metab* (2010).doi:10.1016/j.tem.2010.06.009
15. Franklin, R.J.M. & ffrench-Constant, C. Remyelination in the CNS: from biology to therapy. *Nat. Rev. Neurosci* **9**, 839-855 (2008).
16. Schrage, K., Koopmans, G., Joosten, E.A.J. & Mey, J. Macrophages and neurons are targets of retinoic acid signaling after spinal cord contusion injury. *Eur. J. Neurosci* **23**, 285-295 (2006).
17. Cahoy, J.D. et al. A transcriptome database for astrocytes, neurons, and oligodendrocytes: a new resource for understanding brain development and function. *J. Neurosci* **28**, 264-278 (2008).
18. Krezel, W. et al. RXR gamma null mice are apparently normal and compound RXR alpha +/-/RXR beta -/-/RXR gamma -/- mutant mice are viable. *Proc. Natl. Acad. Sci. U.S.A* **93**, 9010-9014 (1996).
19. Haugen, B.R. et al. Retinoid X receptor gamma-deficient mice have increased skeletal muscle lipoprotein lipase activity and less weight gain when fed a high-fat diet. *Endocrinology* **145**, 3679-3685 (2004).
20. Brown, N.S. et al. Thyroid hormone resistance and increased metabolic rate in the RXR-gamma-deficient mouse. *J. Clin. Invest* **106**, 73-79 (2000).
21. Krzyżosiak, A. et al. Retinoid X Receptor Gamma Control of Affective Behaviors Involves Dopaminergic Signaling in Mice. *Neuron* **66**, 908-920 (2010).
22. Takahashi, B. et al. Novel retinoid X receptor antagonists: specific inhibition of

retinoid synergism in RXR-RAR heterodimer actions. *J. Med. Chem* **45**, 3327-3330 (2002).
23. Heyman, R.A. et al. 9-cis retinoic acid is a high affinity ligand for the retinoid X receptor. *Cell* **68**, 397-406 (1992).
24. Pombo, P.M., Barettino, D., Ibarrola, N., Vega, S. & Rodríguez-Peña, A. Stimulation of the myelin basic protein gene expression by 9-cis-retinoic acid and thyroid hormone: activation in the context of its native promoter. *Brain Res. Mol. Brain Res* **64**, 92-100 (1999).
25. Kagechika, H. & Shudo, K. Synthetic retinoids: recent developments concerning structure and clinical utility. *J. Med. Chem* **48**, 5875-5883 (2005).
26. Nishimaki-Mogami, T. et al. The RXR agonists PA024 and HX630 have different abilities to activate LXR/RXR and to induce ABCA1 expression in macrophage cell lines. *Biochem. Pharmacol* **76**, 1006-1013 (2008).
27. Birgbauer, E., Rao, T.S. & Webb, M. Lysolecithin induces demyelination in vitro in a cerebellar slice culture system. *J. Neurosci. Res* **78**, 157-166 (2004).
28. Klemann, C. et al. Synthetic retinoid AM80 inhibits Th17 cells and ameliorates experimental autoimmune encephalomyelitis. *Am. J. Pathol* **174**, 2234-2245 (2009).
29. Sim, F.J., Zhao, C., Penderis, J. & Franklin, R.J.M. The age-related decrease in CNS remyelination efficiency is attributable to an impairment of both oligodendrocyte progenitor recruitment and differentiation. *J. Neurosci* **22**, 2451-2459 (2002).
30. Moreno, S., Farioli-Vecchioli, S. & Cerù, M.P. Immunolocalization of peroxisome proliferator-activated receptors and retinoid X receptors in the adult rat CNS. *Neuroscience* **123**, 131-145 (2004).
31. Sim, F.J. et al. Complementary patterns of gene expression by human oligodendrocyte progenitors and their environment predict determinants of progenitor maintenance and differentiation. *Ann. Neurol* **59**, 763-779 (2006).
32. Altucci, L., Leibowitz, M.D., Ogilvie, K.M., de Lera, A.R. & Gronemeyer, H. RAR and RXR modulation in cancer and metabolic disease. *Nat Rev Drug Discov* **6**, 793-810 (2007).
33. Trousson, A. et al. 25-hydroxycholesterol provokes oligodendrocyte cell line apoptosis and stimulates the secreted phospholipase A2 type IIA via LXR beta and PXR. *J. Neurochem* **109**, 945-958 (2009).
34. Granneman, J., Skoff, R. & Yang, X. Member of the peroxisome proliferator-activated receptor family of transcription factors is differentially expressed by oligodendrocytes. *J. Neurosci. Res* **51**, 563-573 (1998).
35. Almad, A. & McTigue, D.M. Chronic expression of PPAR-delta by oligodendrocyte lineage cells in the injured rat spinal cord. *J. Comp. Neurol* **518**, 785-799 (2010).
36. Diab, A. et al. Ligands for the peroxisome proliferator-activated receptor-gamma and the retinoid X receptor exert additive anti-inflammatory effects on experimental autoimmune encephalomyelitis. *J. Neuroimmunol* **148**, 116-126 (2004).
37. Du, P., Kibbe, W.A. & Lin, S.M. lumi: a pipeline for processing Illumina microarray. *Bioinformatics* **24**, 1547-1548 (2008).
38. Georgiades, P. & Brickell, P.M. Differential expression of the rat retinoid X receptor gamma gene during skeletal muscle differentiation suggests a role in myogenesis. *Dev. Dyn* **210**, 227-235 (1997).
39. McCarthy, K.D. & de Vellis, J. Preparation of separate astroglial and

oligodendroglial cell cultures from rat cerebral tissue. *J. Cell Biol* **85**, 890-902 (1980).
40. Laursen, L.S., Chan, C.W. & ffrench-Constant, C. An integrin-contactin complex regulates CNS myelination by differential Fyn phosphorylation. *J. Neurosci* **29**, 9174-9185 (2009).

# Supplementary Information Titles

*Please list each supplementary item and its title or caption, in the order shown below. Please include this form at the end of the Word document of your manuscript or submit it as a separate file.*

**Note that we do NOT copy edit or otherwise change supplementary information, and minor (nonfactual) errors in these documents cannot be corrected after publication.** Please submit document(s) exactly as you want them to appear, with all text, images, legends and references in the desired order, and check carefully for errors.

**Journal:** Nature Neuroscience

| | |
|---|---|
| **Article Title:** | Retinoid X receptor gamma signaling accelerates CNS remyelination |
| **Corresponding Author:** | Robin J.M. Franklin |
| | |

| Supplementary Item & Number **(add rows as necessary)** | Title or Caption |
|---|---|
| Supplementary Figure 1 | Graphical analysis of IPA identified genes associated with RXR signaling |
| Supplementary Figure 2 | RXR expression in remyelinating lesions |
| Supplementary Figure 3 | Decreased oligodendrocyte differentiation after RXR knockdown |
| Supplementary Figure 4 | Full length blot showing siRNA knockdown of RXR-α and RXR-γ |
| Supplementary Figure 5 | RXR-γ null mouse analysis |
| Supplementary Figure 6 | Decreased oligodendrocyte differentiation after RXR antagonist treatment |
| Supplementary Figure 7 | Apoptosis and proliferation count |
| Supplementary Table 1 | Total genes differentially expressed between 5, 14 and 28 days post CCP demyelination |
| Supplementary Table 2 | Gene list used for IPA analysis |
| Supplementary Table 3 | Active signaling networks found between 5 and 14 dpl |
| Supplementary Table 4 | Total genes differentially expressed between 5 and 14 dpl ($P < 0.05$) used for volcano plot |
| Supplementary Table 5 | Assessment of known nuclear receptors in the CNS remyelination transcriptome |

| | |
|---|---|
| Supplementary Table 6 | IPA identified RXR associated pathways from the remyelination transcriptome |
| Supplementary Table 7 | MS cases used for the study |

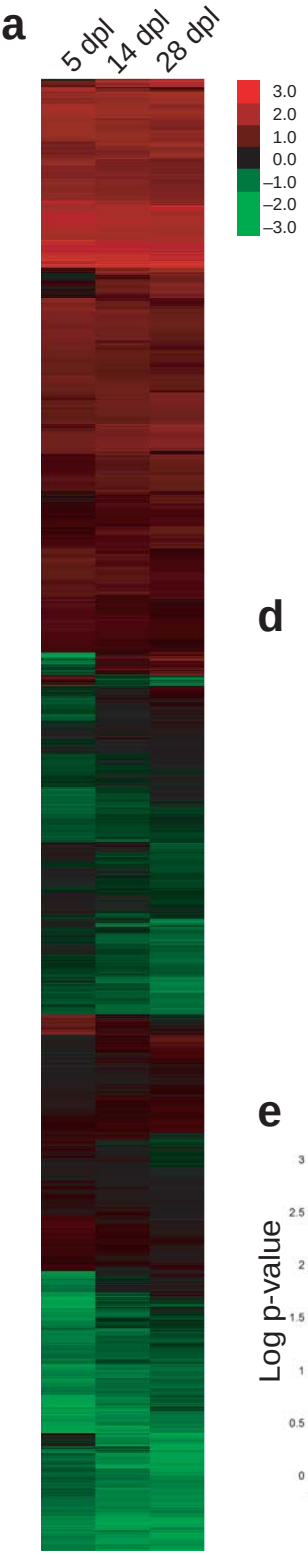


**b**

| Up at 14 vs 5dpl | Fold Change | Up at 28 vs 14dpl | Fold Change |
|---|---|---|---|
| *Sostdc1* | 7.99872704 | *Cdc2* | 4.132710966 |
| *Tspan2* | 7.54935374 | *Ccnb2* | 4.026117318 |
| *Mal* | 7.20167234 | *Prc1* | 3.877652669 |
| *Edg2* | 6.8640735 | *Kif11* | 3.551185008 |
| *Rxrg* | 6.7504494 | *Cdkn3* | 3.353299344 |
| *Mobp* | 6.50949408 | *Cks2* | 3.277683674 |
| *Mog* | 6.48159998 | *Aurkb* | 3.117252074 |
| *Scn6a* | 6.4672945 | *Nrp1* | 3.062468367 |
| *Pmp22* | 6.24930808 | *Spbc24* | 3.055241893 |
| *Dhh* | 5.80567638 | *Traf4af1* | 3.041355091 |

| Up at 5 vs 14dpl | Fold Change | Up at 14 vs 28dpl | Fold Change |
|---|---|---|---|
| *Mmp7* | 7.6457323 | *Hapln2* | 5.804108944 |
| *Cxcl13* | 5.81214896 | *Ermn* | 4.240754546 |
| DIgR1 | 5.60482072 | *Klk6* | 4.064896881 |
| *Selp* | 5.58922846 | *Aldh1a1* | 3.900766502 |
| *Cd300le* | 5.50162194 | *Mal* | 3.606715879 |
| *Cd36* | 5.39107916 | *Ppp1r14a* | 3.475169663 |
| *Plac8* | 5.29770612 | *Spock1* | 3.442572894 |
| *Arg1* | 5.0592168 | *Chi3l1* | 3.406972927 |
| *Igsf7* | 5.0250304 | *Mog* | 3.371213385 |
| *Bst1* | 4.91906184 | *Car2* | 3.357460537 |

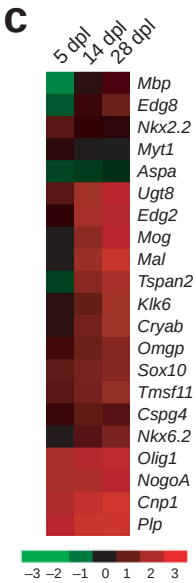


**d**

| Up at 5 vs 14 | Number of Molecules | P-value |
|---|---|---|
| Cell-mediated Immune Response | 115 | 4.86E-27 – 7.05E-06 |
| Tissue Development | 86 | 3.37E-26 – 8.72E-06 |
| Humoral Immune Response | 80 | 1.74E-25 – 5.85E-07 |
| Hematological System Development and Function | 91 | 6.95E-24 – 9.83E-06 |
| Immune Cell Trafficking | 63 | 6.95E-24 – 7.05E-06 |
| **Up at 14 vs 5** | | |
| Nervous System Development and Function | 114 | 6.26E-19 – 3.09E-04 |
| Lymphoid Tissue Structure and Development | 108 | 6.26E-19 – 3.71E-05 |
| Tissue Development | 100 | 1.09E-17 – 1.92E-04 |
| Cell-mediated Immune Response | 76 | 7.49E-14 – 2.60E-04 |
| Organismal Survival | 62 | 1.30E-12 – 2.67E-05 |
| **Up at 28 vs 14** | | |
| Nervous System Development and Function | 131 | 3.08E-10 – 1.79E-03 |
| Cell-mediated Immune Response | 78 | 3.69E-10 – 3.86E-04 |
| Behavior | 48 | 5.32E-10 – 1.31E-03 |
| Lymphoid Tissue Structure and Development | 42 | 2.44E-08 – 1.73E-03 |
| Tissue Development | 87 | 2.50E-08 – 1.50E-03 |

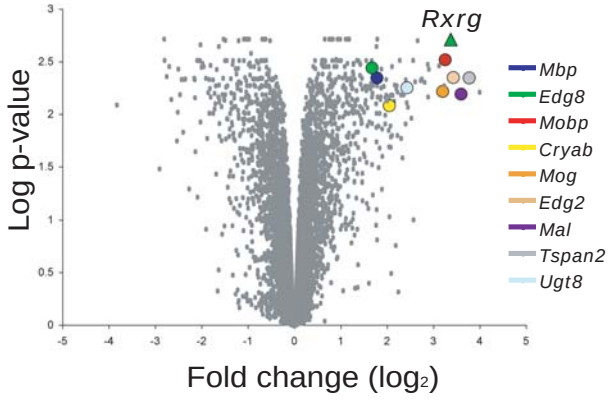


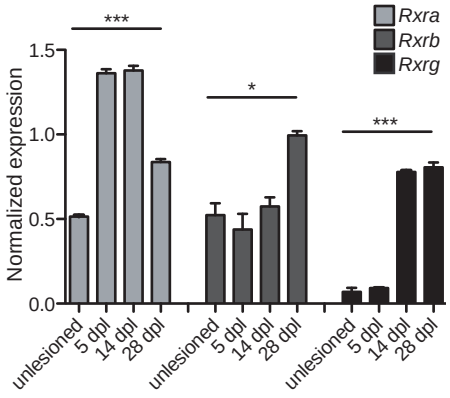


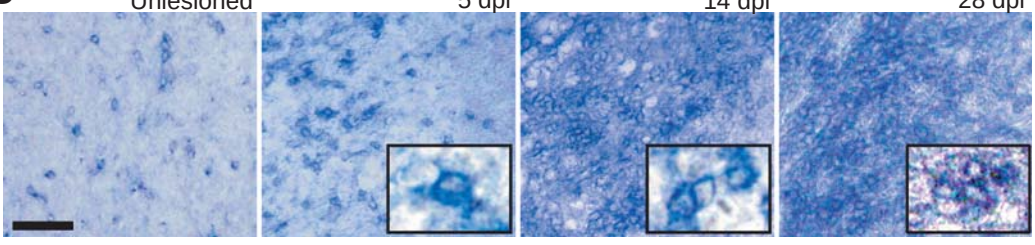


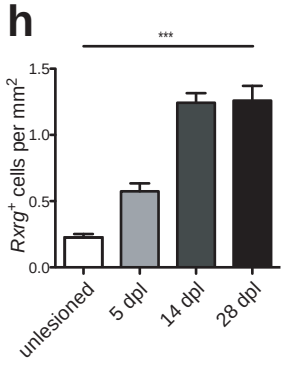


Figure-1 (Franklin)

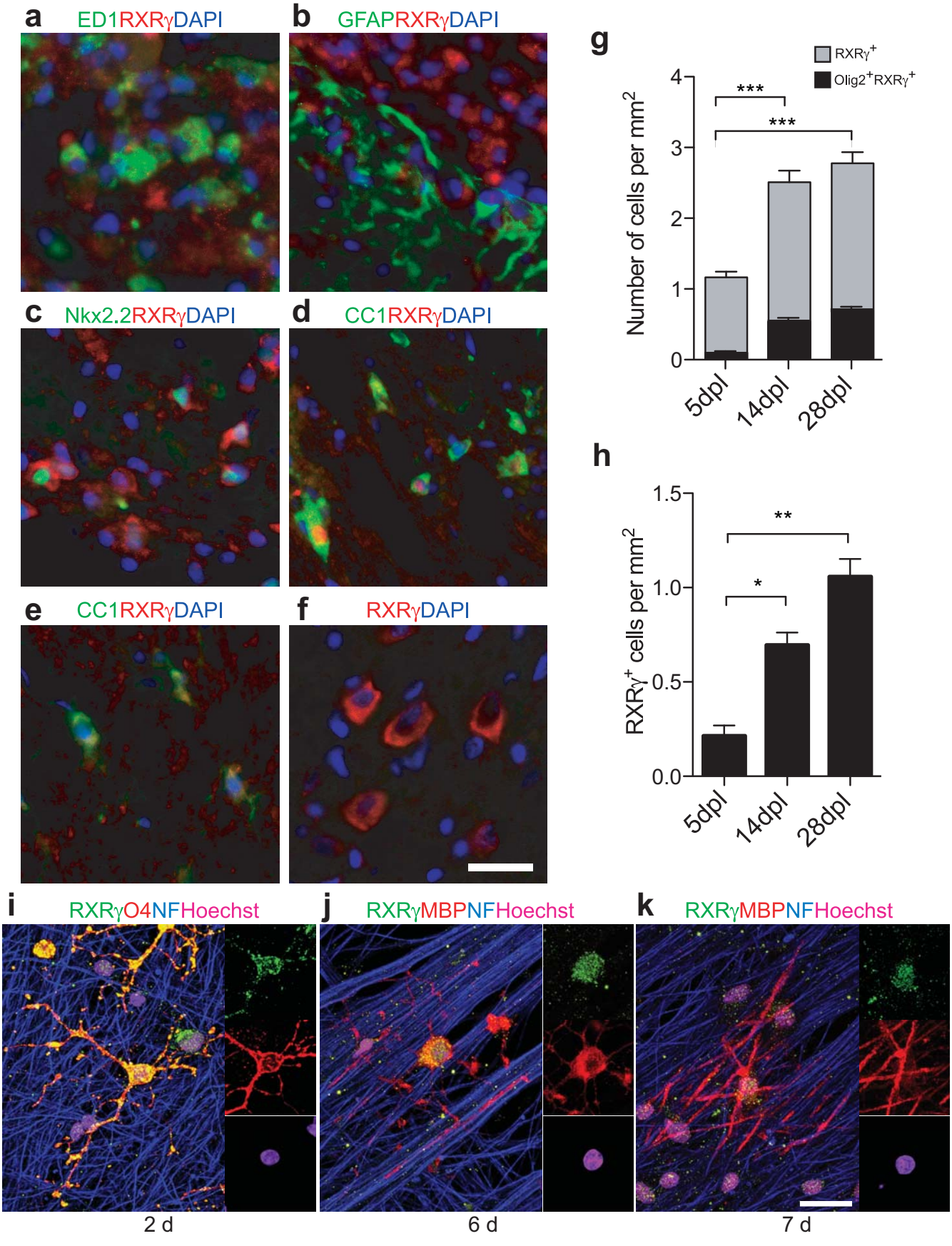
a
ED1RXRγDAPI
b
GFAPRXRγDAPI
c
Nkx2.2RXRγDAPI
d
CC1RXRγDAPI
e
CC1RXRγDAPI
f
RXRγDAPI
g
RXRγ+
Olig2+RXRγ+
Number of cells per mm2
***
***
0
1
2
3
4
5dpl
14dpl
28dpl
h
RXRγ+ cells per mm2
**
*
0.0
0.5
1.0
1.5
5dpl
14dpl
28dpl
i
RXRγO4NFHoechst
j
RXRγMBPNFHoechst
k
RXRγMBPNFHoechst
2 d
6 d
7 d

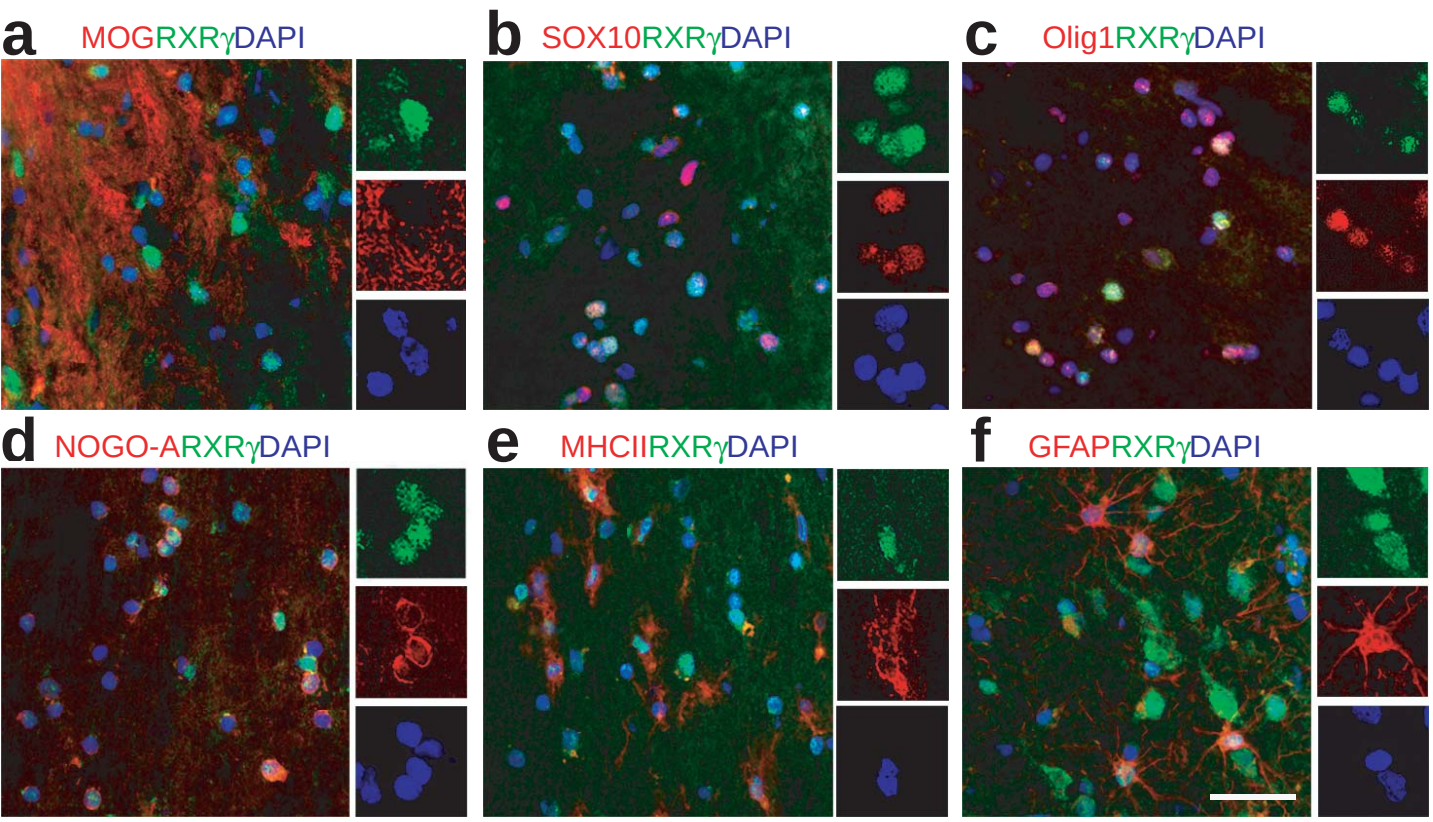


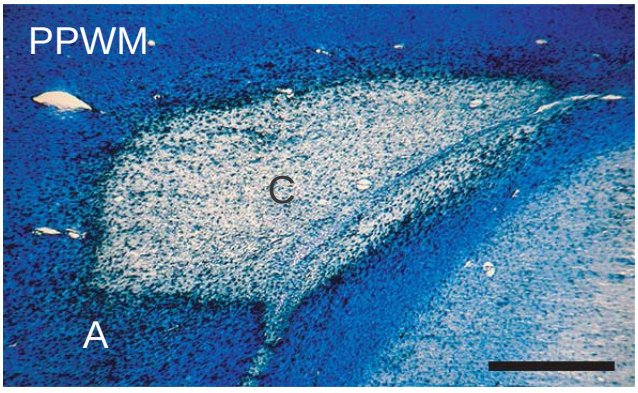


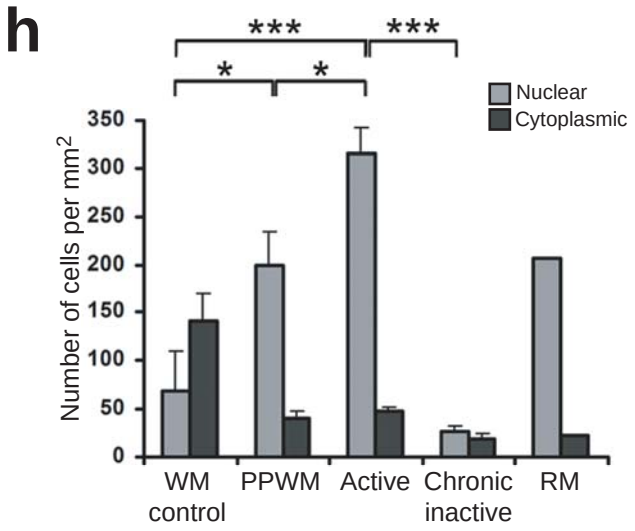


Figure-3 (Franklin)

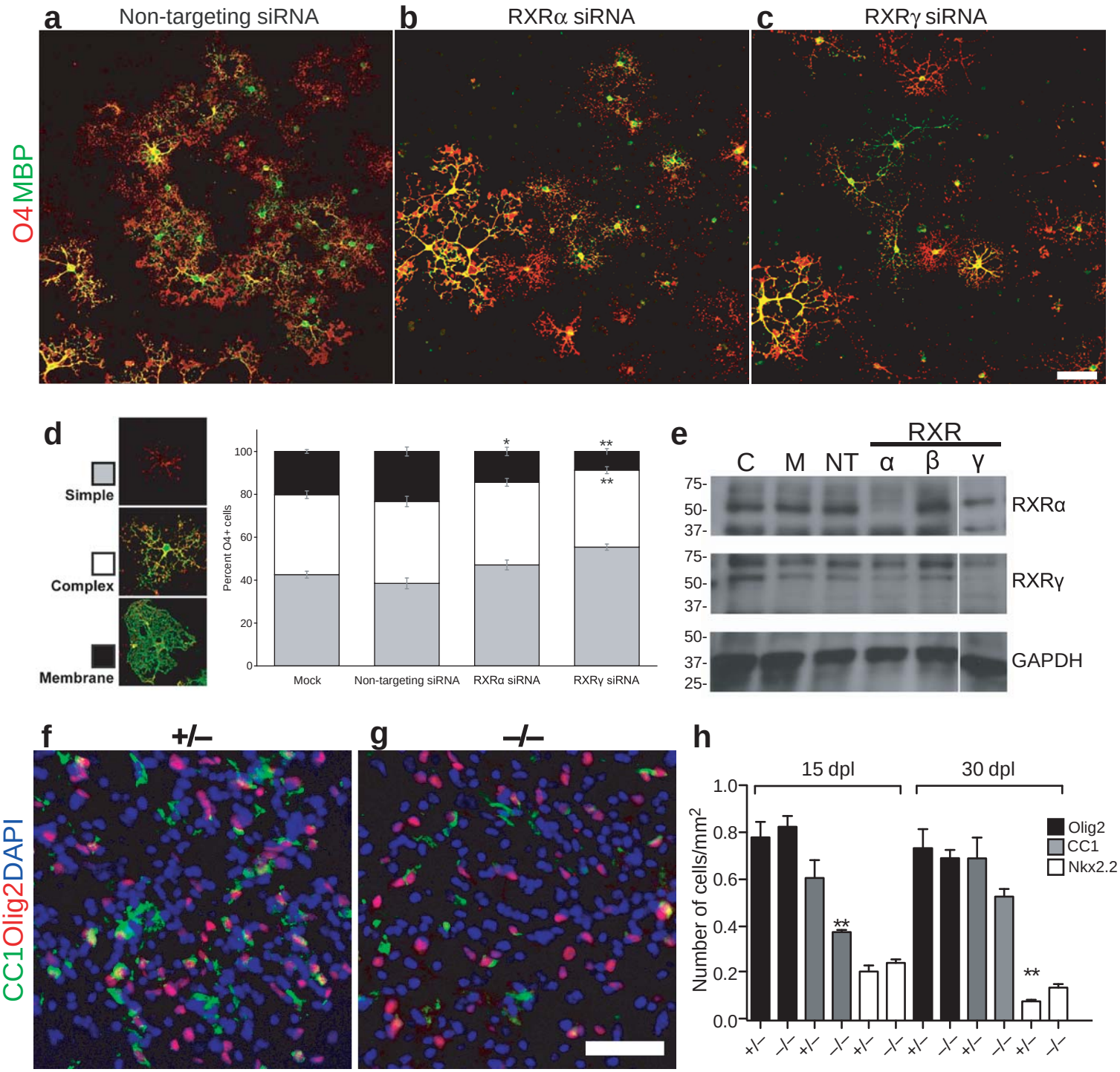


Figure-4 (Franklin)

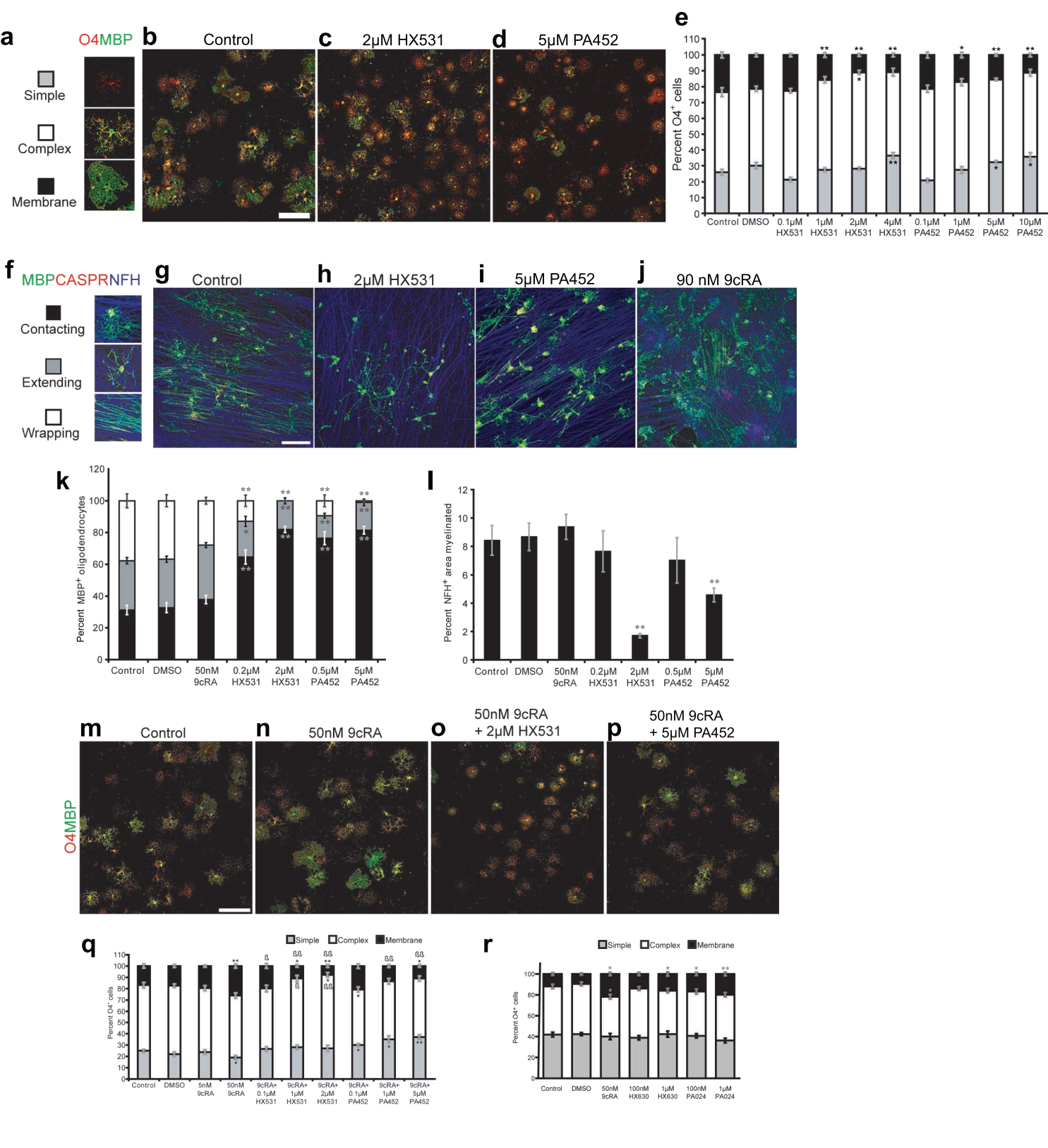


Figure-5 (Franklin)

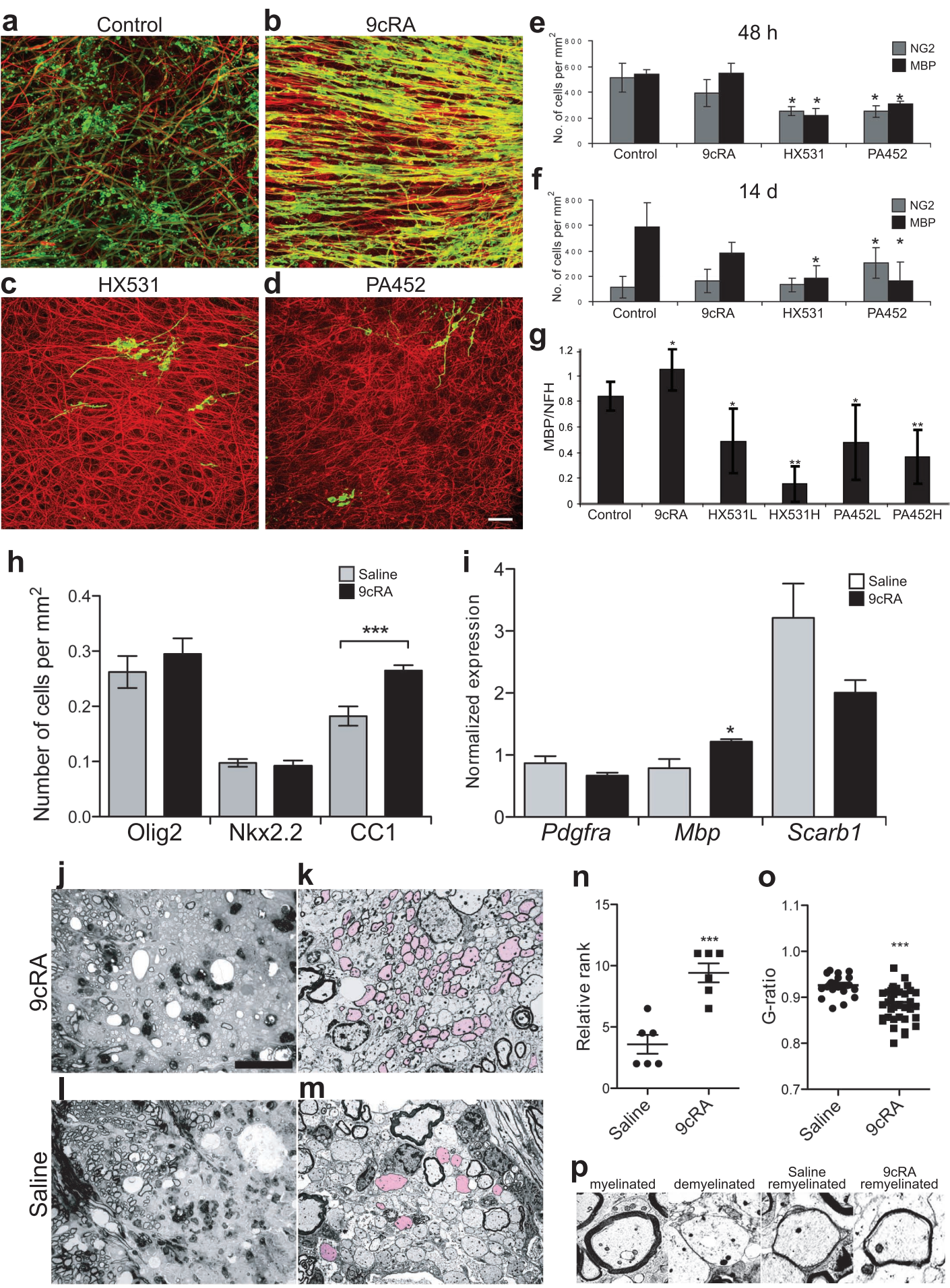


Figure-6 (Franklin)

| RXR pathways | -Log (P-value) | Ratio | Genes |
|---|---|---|---|
| LXR/RXR Activation | 1.12E01 | 4.49E-01 | IL1A, LCAT, CCL7, TNFRSF11B, RELA, HADH, LPL, RXRA, CD14, CD36, SREBF1, ECHS1, NGFR, HMGCR, LBP, IL1R2, TNFRSF1A, RXRB, NCOR1, NR1H2, MMP9, TLR4, IL18, CCL2, APOC1, ABCG1, APOE, IRF3, RXRG, IL1B, NR1H3 |
| VDR/RXR Activation | 1.22E01 | 4.81E-01 | TGFB2, PRKCH, GADD45A, PRKCD, CEBPA, RXRA, HES1, IL12A, GTF2B, CD14, PRKCZ, PRKCA, PRKCE, PRKCQ, TRPV6, KLK6, IGFBP6, CALB1, PDGFA, PRKCB, HR, PSMC5, CXCL10, YY1, RXRB, FOXO1, SPP1, NCOR1, CCL5, CEBPB, CDKN1B, CSNK2A1, KLF4, CYP24A1, CCNC, RXRG, IGFBP3 |
| LPS/IL-1 Mediated Inhibition of RXR Function | 1.42E01 | 3.32E-01 | ALDH1A2, TNFRSF11B, SOD3, ABCB1, RXRA, CPT1A, GSTT1, GSTM1, ALDH3B1, NGFR, ACOX1, IL1R2, CES2, MYD88, NR1H2, TLR4, SLC27A1, APOC1, APOE, MAP3K1, FABP7, XPO1, SCARB1, ACSL4, ACSL3, FMO4, RARA, NDST1, MAOA, IL1B, NR1H3, CPT2, MAOB, ABCB9, HMGCS2, FABP3, SULT1A1, CD14, ALDH3A2, SREBF1, GSTK1, MGMT, CAT, GSTO1, ALDH1A1, LBP, ABCC3, ACSL5, ACSL6, TNFRSF1A, HS3ST1, CHST10, GSTM3, GSTP1, ALDH9A1, JUN, ABCG1, MGST1, ACSL1, GSTT2, FABP4, HMGCS1 |
| PPARα/RXR Activation | 1.74E01 | 3.86E-01 | TGFB2, ADCY3, GPD2, GNA11, SMAD4, PRKAR1A, CAND1, ADCY4, RXRA, PRKCA, TGFB1, PLCB3, NFKBIA, TGFBR2, MAPK14, NRAS, ACOX1, IL1R2, PRKCB, PRKAG1, PRKACA, PLCB1, MAPK1, STAT5B, MAP2K6, PRKAR2B, RAF1, TGFBR1, SLC27A1, NFKBIB, ACVR2B, PDIA3, ACADL, PLCG2, IL1B, MAPK3, RELA, LPL, ADCY5, HSP90AA1, MAP2K2, SMAD2, ADCY2, PRKAG2, CD36, PLCD4, PLCG1, GOT2, PRKAA1, MRAS, SHC1, KRAS, ADCY8, ACAA1, IKBKB, PLCL1, NCOR1, GPD1, JAK2, JUN, NCOA6, MAP2K1, PLCD1, PLCB2 |
| CAR/RXR Activation | 2.16E00 | 3.1E-01 | SULT1A1, ABCC3, RXRB, MCL1, CCND1, ABCB1, GADD45B, ALDH1A1, RXRA |
| FXR/RXR Activation | 2.69E00 | 2.41E-01 | IL1A, FOXO1, MAPK12, SDC1, VLDLR, RXRA, IL18, AKT1, CYP27A1, SREBF1, SLC4A2, APOE, CYP8B1, SCARB1, PON1, RARA, G6PC3, ABCB4, IL1B, NR1H3 |
| PXR/RXR Activation | 3.74E00 | 2.79E-01 | ABCC3, CES2, PRKAG1, PRKACA, ABCB9, HMGCS2, FOXO1, PRKAR1A, RELA, ABCB1, PRKAR2B, RXRA, AKT1, CPT1A, PRKAG2, GSTM1, ALDH3A2, NR3C1, ALDH1A1 |
| TR/RXR Activation | 6.19E00 | 3.49E-01 | KLF9, ME1, THRSP, FRAP1, HIF1A, PFKP, RXRA, PIK3C3, ENO1, SREBF1, RCAN2, TRH, STRBP, UCP2, F10, RXRB, SLC16A3, PIK3CA, NCOR1, THRB, THRA, AKT1, PIK3CB, NRGN, HDAC3, NCOA6, PIK3R2, SCARB1, RXRG |

**Table 1.** Genes associated with RXR signaling during remyelination